CHAPTER TWO

Molecular attochemistry: Correlated electron dynamics driven by light

Peter Saalfrank[a,*], Florian Bedurke[a], Chiara Heide[a], Tillmann Klamroth[a], Stefan Klinkusch[a], Pascal Krause[b], Mathias Nest[a], and Jean Christophe Tremblay[c]

[a]Universität Potsdam, Institut für Chemie, Potsdam, Germany
[b]Freie Universität Berlin, Institut für Chemie und Biochemie, Berlin, Germany
[c]Laboratoire de Physique et Chimie Théoriques, UMR7019, CNRS-Université de Lorraine, Metz, France
*Corresponding author: e-mail address: peter.saalfrank@uni-potsdam.de

Contents

Advances in Quantum Chemistry, Volume 81
ISSN 0065-3276
https://doi.org/10.1016/bs.aiq.2020.03.001

Abstract

Modern laser technology and ultrafast spectroscopies have pushed the timescales for detecting and manipulating dynamical processes in molecules from the picosecond over femtosecond domains, to the attosecond regime (1 as $= 10^{-18}$ s). This way, real-time dynamics of electrons after their photoexcitation can be probed and manipulated. In particular, experiments are moving more and more from atomic and solid state systems to molecules, opening the fields of "molecular electron dynamics" and "attosecond chemistry." Also on the theory side, powerful quantum dynamical tools have been developed to rationalize experiments on ultrafast electron dynamics in molecular species.

In this contribution, we concentrate on theoretical aspects of ultrafast electron dynamics in molecules, mostly driven by lasers. The dynamics will be described with the help of wavefunction-based ab initio methods such as time-dependent configuration interaction (TD-CI) or the multiconfigurational time-dependent Hartree-Fock (MCTDHF) methods. Besides a survey of the methods and their extensions toward, e.g., treatment of ionization, laser pulse optimization, and open quantum systems, two specific examples of applications will be considered: The creation and/or dynamical fate of electronic wavepackets, and the nonlinear optical response to laser pulse excitation in molecules by high harmonic generation (HHG).

1. Prologue

This contribution is based on a lecture "Molecules driven by light: Electron and nuclear dynamics" given by one of us (PS) at the 10th Triennal Congress of the International Society for Theoretical Chemical Physics (ISTCP), held at Tromsø, Norway, from July 11—17, 2019. The founder of the ISTCP, Janos Ladik, was the "Doktorvater" (PhD advisor) of PS from 1988 to 1991, in Erlangen, Germany. Sadly, Janos passed away on March 17, 2018, still active as a scientist up into his late years. One of the sessions at ISTCP 2019, the "Ladik symposium," was devoted to the memory of Janos Ladik.

The author of this paper (PS) remembers quite well some of the vivid activities taking place at the Chair of Theoretical Chemistry in Erlangen in the late 1980s, which were connected to the foundation of the ISTCP. Frankly, most of the group members were a bit skeptical at the time—why another society, when so many existed already? Janos insisted that there was a gap, however, precisely when it came to representing the field of Theoretical Chemical Physics, "his field." Theoretical Chemical Physics was strongly expanding at the time and continues to do so up to the present days—also in the form of popular offsprings like "Computational Chemistry,"

"Computational Materials Science" or "Molecular Modeling." In retrospect, Janos Ladik had a keen instinct also here, like in many other instants as well. In fact, here we are, 30 years later, with the ISTCP hosting thousands of scientists who feel as "Theoretical Chemical Physicists," celebrating the 10th meeting of the Society.

Some of the parallel sessions at ISTCP 2019 impressively represent areas where Ladik acted as a scientific pioneer. One of the sessions was about "Heavy-element chemistry," i.e., relativistic quantum chemistry. Ladik was one of the first to study relativistic effects (even including quantum electrodynamical corrections) for molecules, back in the 1950s. Another field was the formulation and application of wavefunction theory (WFT; semiempirical, Hartree-Fock, and post-Hartree Fock) to periodic solids, e.g., polymers. For some time, periodic density functional theory (DFT) seemed to be the only practical way to treat periodic systems but recent years have witnessed a strong renaissance of correlated WFT, due to enormous progress in the field of which some were presented in ISTCP 2019 in the "Emergent electronic structure" and "Large-scale electronic structure" sessions. Finally, the "Computational biophysics" session was about research for which Ladik contributed to many concepts and ideas—sometimes too early for his time. Using quantum mechanical methods, he worked on charge, energy, and soliton transport in biopolymers, on the electronic structure of DNA and proteins, and on a quantum theory of aging and cancer—long before others finally joined in, both from the theory and the experimental sides. Janos was always interested in fundamental questions but also in very practical problems if he considered them important—his interest in cancer theory and high-T_c superconductivity are only two examples. He had the vision and strength, to bring seemingly totally unrelated phenomena/methods/concepts together to create something new, unexpected. Again in retrospect, this may be the reason why sometimes his ideas where not acknowledged as much as they should—certainly not at the time they were emerging.

The following contribution is devoted to Janos Ladik, a visionary scientist, a caring advisor, and an influential promoter of Theoretical Physical Chemistry in general.

2. Introduction

Molecules interacting with light play the central role in *photochemistry*, i.e., the photoinduced breaking and making of bonds, and also in *photophysics*, i.e., in photoinduced processes where molecular motions are induced that are less "violent" and leave the molecule more or less intact.

An incomplete list of examples of the former contains photoisomerizations, photodissociation, photosynthesis, electro- and pericyclic reactions, and photocatalysis. Examples of the latter are all sorts of molecular spectroscopies, nonradiative processes after photoexcitation (by Internal Conversion, IC, or Intersystem Crossing, ISC), photoionization, and the emission of radiation after excitation, e.g., in organic light emitting diodes (OLEDs), in the form of bioluminescence, or by high harmonic generation (HHG). Different processes during and after photoexcitation proceed on different timescales, starting from attoseconds (10^{-18} s) when electrons are set in motion while nuclei are still at rest, over femtoseconds (10^{-15} s), when nuclei start to move within the molecule, to picoseconds, nanoseconds and longer when "slow" molecular motions (such as low-frequency vibrations or rotations) come into play. These timescales can be monitored by various forms of time-resolved spectroscopies. Recent remarkable progress in experimental laser spectroscopy has pushed the resolvable timescale from the femtosecond regime, well into the attosecond, i.e., electronic, regime.[1] While "femtochemistry" is well established in the molecular world since about three decades,[2] "attochemistry," or, more general, "molecular attoscience" is only emerging. In fact, the main focus of attoscience was on atoms (and also on surfaces) so far, while "molecular attoscience" is more recent.

In the contribution of PS at ISTCP 19 entitled "Molecules driven by light: Electron and nuclear dynamics" many aspects of (i) pure electron dynamics, (ii) spectroscopy and photophysics in a time-dependent context, and (iii) photochemistry (for light-induced cis-trans isomerizations) were covered. In the current paper, we focus on the former, i.e., on ultrafast, pure electron dynamics in molecules. Specifically, the paper describes some of our contributions toward the time-resolved theory of photoinduced electron dynamics in excited molecules, using correlated, systematically improvable wavefunction methods. Also two classes of applications will be touched upon, namely the creation and fate of electronic wavepackets in molecular systems, and HHG in molecules. As stated in both cases, only electronic motion will be considered, by invoking the fixed-nuclei approximation. Naturally, the material selected for this paper is biased toward the activities of the Potsdam group in recent years, both in methodology and applications. We cannot and also do not make the attempt to review all the wonderful theoretical work done by others in this field.

The paper is organized as follows. In Section 3, general aspects of molecules interacting with laser pulses with emphasis on electronic wavepackets and nonlinear molecular response through HHG will be summarized.

In Section 4, we review wavefunction-based methods used by our group in recent years, namely time-dependent configuration interaction (TD-CI) and multiconfigurational time-dependent Hartree-Fock (MCTDHF). In Section 5, several extensions in particular of the TD-CI method will be highlighted, namely ways to treat random molecular orientations, ways to design laser pulses for desired purposes, ways to treat ionization losses, and, finally, how to include energy and phase relaxation in "open" quantum systems. In Section 6, as a first set of applications electronic wavepacket dynamics will be considered, and in Section 7 HHG in molecular systems as a second one. A final Section 8 summarizes and concludes this work.

3. Electron dynamics in molecules: From wavepackets to HHG

When laser pulses interact with molecules, complete state-to-state transitions from a singlet ground state, S_0 say, to an excited singlet state, S_n, may be enforced by so-called π-pulses. Under the semiclassical dipole approximation, which treats the field classically and neglects the coordinate-dependence of the electric field and magnetic interactions, the π-pulse condition for a pulse of the form

$$\underline{F}(t) = \underline{F}_0\, s(t)\, \cos(\omega_0 t) \tag{1}$$

is given, under the so-called rotating wave approximation, as

$$\underline{\mu}_{0n}\underline{F}_0 \int_{-\infty}^{\infty} s(t)dt = \hbar\pi. \tag{2}$$

Here, $\underline{F} = (F_x, F_y, F_z)$ is the electrical field vector, $\underline{F}_0 = (F_{x0}, F_{y0}, F_{z0})$ contains the maximal amplitudes, $\omega_0 = (E_n - E_0)/\hbar$ is a carrier frequency, resonant with the desired transition (E_n and E_0 are final and initial state energies), and $s(t)$ a temporal shape function (see below). Further, $\underline{\mu}_{0n} = \langle \Psi_0 | \underline{\hat{\mu}} | \Psi_n \rangle$ is the transition dipole moment connecting state 0 (with electronic wavefunction Ψ_0), with state n (with Ψ_n), and $\underline{\hat{\mu}} = -\sum_{i=1}^{N} \underline{r}_i + \sum_{A=1}^{N_A} Z_A \underline{R}_A$ the dipole operator for a molecule with N electrons ($\underline{r}_i$ is the spatial coordinate of electron i) and N_A nuclei (at positions $\underline{R}_A$) with charges $+Z_A$. We use atomic units throughout if not indicated otherwise but $\hbar$ is always explicitly indicated for convenience. If the pulses either (i) do *not*

fulfill the π-pulse condition, (ii) and/or if the pulses are temporaly so short that they become spectrally broad and hit other final states as well, and/or (iii) if they are intense such that multiphoton processes come into play, an *electronic wavepacket*,

$$\Psi(t) = \sum_n C_n(t_0)\ e^{-iE_n(t-t_0)/\hbar}\ \Psi_n \tag{3}$$

is created, i.e., a linear combination of eigenstates Ψ_n of the (field-free) electronic Hamiltonian $\hat{H}_0$ (see below) with energies E_n and probability amplitudes $C_n(t_0)$. Here, t_0 is a certain reference time after the pulse. In contrast to stationary eigenstates of $\hat{H}_0$, the nonstationary electronic wavepacket comes with rich dynamics, e.g., the molecular dipole moment $\underline{\mu} = \langle\Psi(t)|\underline{\hat{\mu}}|\Psi(t)\rangle$ can be oscillating with time, even after the pulse is off. The oscillating dipole, on the other hand, can cause the emission of radiation, leading e.g., to HHG.[3]

HHG has been studied a lot in the past, as a source of coherent XUV/soft X-ray radiation[4] or for creating attosecond pulses.[1,5,6] First realized for solids or monatomic gases, HHG was later observed in diatomic[7,8] and three-atomic molecules (e.g., CO_2[7,9] and N_2O[9]), and, more recently, for polyatomic complex organic or biomolecules.[10–12] This opens the way to *molecular HHG spectroscopy*. For instance, in Ref. 10 it was suggested to use HHG from linearly polarized lasers, to discriminate different configurational organic isomers. Specifically, it was claimed that the cis- and trans-isomers of 1,2-dichloroethene (DCE) can be distinguished in this way, even when the molecules are *randomly oriented*.

Besides experimental progress, also the quantum mechanical modeling of molecular HHG spectra and of many-electron dynamics in general, was greatly advanced recently, by a broad variety of quantum mechanical methods. Here we largely focus on Wavefunction Theory (WFT), where the methods range from numerically accurate solutions of the time-dependent, molecular Schrödinger equation (even including nuclear motion and nonadiabatic effects) for one- and two-electron systems,[13] over time-dependent Hartree-Fock to configuration interaction based approaches.[14–17] Often, the more computationally demanding yet more accurate methods are done in the fixed-nuclei approximation, also because nuclear dynamics is typically much slower than the electron dynamics of interest. As an alternative to WFT, real-time time-dependent density functional theory (RT-TD-DFT) was applied to HHG for CO, N_2, or N_2O.[18,19] In comparison to RT-TD-DFT, correlated wavefunction methods such as TD-CI or

MCTDHF[20–24] have the advantage of being, in principle, systematically improvable. The TD-CI methods at least have the additional advantage of always correctly producing population inversion in two-level systems when driven by π-pulses, or, more generally, properly accounting for Rabi oscillations. In contrast, RT-TD-DFT is not straightforward when trying to realize π-pulses for complete population inversion, to properly describe Rabi oscillations,[25–27] or to apply optimal control theory (OCT, see below),[28,29] all due to the nonlinear equations of motion. Similar problems hold for nonlinear WFT methods, such as MCTDHF. In any case, when using WFT for many-electron systems, in practice one needs to compromise on the chosen level of excitations, on the basis set, and on the treatment of large-amplitude electronic motion and ionization, which typically occur during HHG, for example, when using short-pulse excitations. We shall now review some of the wavefunction-based methods to describe electron dynamics.

4. Time-dependent configuration interaction (TD-CI) and multiconfigurational time-dependent Hartree-Fock (MCTDHF)

4.1 The time-dependent electronic Schrödinger equation

In what follows, we wish to solve a time-dependent electronic Schrödinger equation (TDSE) at fixed nuclear positions to model laser-driven electron dynamics in molecules, in the dipole approximation, i.e.,

$$i\hbar\frac{\partial\Psi(t)}{\partial t} = \left(\hat{H}_0 - \underline{\hat{\mu}}\underline{F}(t)\right)\Psi(t). \tag{4}$$

Here, $\hat{H}_0$ is the field-free electronic Hamiltonian,

$$\hat{H}_0 = -\sum_{i=1}^{N}\frac{\hbar^2}{2}\Delta_i - \sum_{i=1}^{N}\sum_{A=1}^{N_A}\frac{Z_A}{|\underline{r}_i - \underline{R}_A|} + \sum_{i=1}^{N}\sum_{j>i}^{N}\frac{1}{|\underline{r}_i - \underline{r}_j|}. \tag{5}$$

Further, $\underline{\hat{\mu}}$ and $\underline{F}$ are the molecular dipole operator and the field as defined earlier.

4.2 The TD-CI method

As also stated, in Eq. (4), $\Psi(t)$ is the N-electron wavefunction. In the TD-CIS (S=Singles) method, $\Psi(t)$ is expanded with the help of time-independent CIS states,[30] Ψ_n^{CIS}, with energies E_n^{CIS}[31,32]:

$$\Psi(t) = \sum_{n=0}^{L} C_n(t)\; e^{-iE_n^{\mathrm{CIS}}t/\hbar}\; \Psi_n^{\mathrm{CIS}}. \tag{6}$$

In what follows we will sometimes use the restricted closed-shell Hartree-Fock (RHF) ground state Slater determinant $\Psi_0^{\mathrm{HF}} = \Psi_0^{\mathrm{CIS}}$ as the initial wavefunction. Ψ_0^{HF} and spin-adapted singly excited Slater determinants (Configuration State Functions, CSFs), ${}^1\Psi_a^r = \frac{1}{\sqrt{2}}\left(\Psi_a^r - \Psi_{\bar{a}}^{\bar{r}}\right)$, representing pure singlets[33] serve as a basis for constructing the CIS states. Here, Ψ_a^r denotes a Slater determinant obtained from exciting an electron from an occupied "spin-up" orbital a of Ψ_0^{HF} to an unoccupied "spin-up" orbital r. $\Psi_{\bar{a}}^{\bar{r}}$ denotes the same for "down-spin" orbitals.

The TD-CI method can be extended by including higher excitations, for instance double (D) excitations—either perturbatively (leading to TD-CIS (D)), or explicitly, leading to TD-CISD (see, e.g., Refs. 32 and 34). We may quite generally write

$$\Psi(t) = D_0(t)\; \Psi_0^{\mathrm{HF}} + \sum_a \sum_r D_a^r(t)\; \Psi_a^r + \sum_{a<b} \sum_{r<s} D_{ab}^{rs}(t)\; \Psi_{ab}^{rs} + \cdots \tag{7}$$

where we have absorbed the phase factors in the coefficients, $D(t)$. Ψ_0^{HF} is again the HF ground state, Ψ_a^r are all single-excitations created from there, Ψ_{ab}^{rs} are all double excitations, and so forth. An exact, full-CI (FCI) solution of the time-dependent electronic Schrödinger equation is obtained when all (up to N-fold) excitations are included in the CI expansion. Of course, this is only possible for few-electron systems treated with moderately large basis sets. Note that in TD-CI methods, only the expansion coefficients $C_n(t)$ are time-dependent, while the Slater determinants (e.g., Ψ_n^{CIS}) by diagonalizing the CI Hamiltonian in the chosen basis/CI excitation level are time-independent.

4.3 The MCTDHF and TD-CASSCF methods

As an alternative, we can not only choose the expansion coefficients to the Slater determinants but also the Slater determinants themselves (via the single-particle functions contained therein) as explicitly time-dependent. This is the idea of MCTDHF, where the Ansatz for the wavefunction is

$$\Psi(t) = \sum_n A_n(t)\; \Psi_n[\{\chi_{i,n}(t)\}]. \tag{8}$$

To obtain coefficients $A_n(t)$ and single-particle functions/orbitals $\chi_{i,n}$ entering the Slater determinants $\Psi_n(t)$ in MCTDHF, the Dirac–Frenkel time-dependent variational principle is employed as outlined elsewhere.[20–24] Due to the larger variational flexibility of the MCTDHF wavefunction compared to the TD-CI wavefunction, usually less Slater determinants are needed to reach a given level of accuracy. As a drawback, the equations of motion for coefficients and orbitals are coupled, highly nonlinear, and not easy to solve in practice.

Often, MCTDHF is used as an *approximation* to solve the electronic TDSE (similar to truncated CI), by considering only an *active space* with M electrons in L spatial orbitals. This leads to the TD-CASSCF(M,L) methods, in analogy to the CASSCF(M,L) methods of stationary quantum chemistry, where (TD-)CASSCF stands for (time-dependent) complete active space self-consistent field. Like TD-CI, TD-CASSCF has well-defined limiting cases: TD-CASSCF(N,N/2) corresponds to Time-Dependent Hartree-Fock (TD-HF), a single-determinant method with time-dependent orbitals. Further, TD-CASSCF(N,K) corresponds to the FCI solution, where K is the number of primitive basis functions used to represent the single-particle functions (molecular orbitals).

Both for MCTDHF and TD-CI, various primitive basis functions can be used. In our own work, we used grid bases as well as atomic orbital like Gaussian basis sets known from standard quantum chemistry. The reader is referred our previous literature for further information, where also numerical details, e.g., on the time-propagation are given. In passing we also note that also a time-dependent analog of coupled cluster theory (TD-CC) has been suggested for electron dynamics.[35,36]

5. Extending TD-CI: Random molecular orientations, laser pulse control, ionization losses, and dissipation

5.1 Random molecular orientations

In what follows, we will often employ linearly polarized laser pulses. Further, we will consider "aligned" molecules being fixed in space, relative to the polarization axis of the pulse. In many experiments, however, molecules are randomly oriented when hit by the pulse. This can equivalently be described by a molecule hit by laser pulses with different polarizations i, where observables are then averaged over all orientations. Let us rewrite Eq. (1) for the case of a pulse linearly polarized along direction i, i.e.,

$$\underline{F}_i(t) = F_0 \, \underline{P}_i \, s(t) \, \cos\left(\omega_0\left(t - t_p\right) + \phi_{\mathrm{CEP}}\right). \tag{9}$$

$\underline{P}_i$ is the polarization vector, ω_0 the carrier frequency as before (not necessarily resonant with a transition energy), and ϕ_{CEP} the carrier envelope phase (set to 0 in the following if not stated otherwise). For the envelope $s(t)$, we often choose a $\cos^2$-shaped function,

$$s(t) = \begin{cases} \cos^2\left[\dfrac{\pi}{2\sigma}\left(t - t_p\right)\right], & \text{if } |t - t_p| \leq \sigma \\ 0, & \text{if } |t - t_p| > \sigma, \end{cases} \tag{10}$$

with 2σ being the pulse duration, and σ its Full Width at Half Maximum (FWHM). At peak time t_p, the field reaches its maximum amplitude F_0, with a mean intensity $I = \frac{1}{2}\epsilon_0 c F_0^2$ (now in SI units, ϵ_0 being the permittivity of vacuum and c the velocity of light). Note that even with the linearly polarized, analytical pulse form (9) and (10), we have the freedom to choose as *control parameters*, F_0, σ, ω_0 and ϕ_{CEP}, for rational pulse design. For instance, choosing F_0 according to Eq. (2) leads to a π-pulse (for a two-level system if in addition $\hbar\omega$ is resonant with the desired transition). As an alternative, various control algorithms may be used to freely design pulses to achieve a specified goal (see below).

To compute properties of laser-driven molecules in random orientations, e.g., HHG spectra calculated by TD-CIS, we adopt a coherent averaging scheme as outlined elsewhere.[37] As argued there, under the dipole approximation we only need to average over the two angles defining the laser polarization and not over all three Euler angles of the molecular orientation. To represent as many different molecular orientations as possible, the polarization vectors are chosen such that their endpoints are maximally uniformly distributed on the surface of a sphere. This is achieved by a technique called "subdivision of an icosahedron."[38] The application and continuous repetition of this procedure provides sets of 12, 42, 162, 642, … polarization vectors, each with a specific orientation.

5.2 Laser pulse control

Another way to reach a target, e.g., complete population of an excited state from a ground state, preparation of a wavepacket, directed charge transfer, or the control of emitted radiation, is to use nonrational pulse optimization instead. In our own work, we have mainly used two strategies for this purpose, namely *optimal control theory* (OCT)[39–41] and a *stochastic pulse optimization* (SPO) scheme.[17,42]

5.2.1 Optimal control theory

In OCT, we maximize the expectation value of a positive target operator $\hat{O}$ at the end of the control time, t_f, under the two additional conditions that the laser field intensity should be as low as possible and the time-dependent Schrödinger equation must be fulfilled. Thus, the functional

$$J = \langle \Psi(t_f)|\hat{O}|\Psi(t_f)\rangle - \int_0^{t_f} \alpha(t)|\underline{E}(t)|^2 dt - 2\,\mathrm{Re}\left[\int_0^{t_f} \left\langle \Phi(t)\left|\frac{\partial}{\partial t} + \frac{i}{\hbar}(\hat{H}_0 - \underline{\hat{\mu}}\underline{E}(t))\right|\Psi(t)\right\rangle dt\right] \tag{11}$$

is maximized. In this equation, $\Phi(t)$ is a Lagrange multiplier and $\alpha(t)$ a user-specified, positive constraint function. The target operator, $\hat{O}$ is often chosen as a projector on a desired state, described by a target wavefunction Ψ_t, i.e.,

$$\hat{O} = |\Psi_t\rangle\langle\Psi_t|. \tag{12}$$

For instance, Ψ_t can be an excited eigenstate of $\hat{H}_0$, or a wavepacket.

From the condition $\delta J = 0$, in OCT the laser field is obtained from three equations, which one solves iteratively. The first one is the Schrödinger equation (4), the other two are

$$i\hbar\frac{\partial\Phi(t)}{\partial t} = \left(\hat{H}_0 - \underline{\hat{\mu}}\underline{E}(t)\right)\Phi(t) \quad \text{with} \quad \Phi(t_f) = \hat{O}\Psi(t_f) \tag{13}$$

and

$$\underline{E}(t) = -\frac{1}{\alpha(t)}\,\mathrm{Im}\left[\langle\Phi(t)|\underline{\hat{\mu}}|\Psi(t)\rangle\right]. \tag{14}$$

Eq. (4) is solved by forward propagation from an initial condition $\Psi(t_0)$ and Eq. (13) by backward propagation with the initial condition $\Phi(t_f) = \hat{O}\Psi(t_f)$. The field is calculated from Eq. (14) at each iteration. The procedure is ideally repeated until convergence is achieved.

Note that this algorithm controls the outcome of electron dynamics only at a given endtime, t_f. Alternative schemes with time-dependent targets are known.[43] Also, the extension of the OCT scheme for dissipative media (open quantum systems) is possible.[44,45]

5.2.2 Stochastic pulse optimization

In the SPO scheme when applied to electron dynamics,[17] the laser pulse in case of linear polarization (polarization direction $\hat{\imath}$), is represented as a truncated Fourier series as

$$F_i(t) = s(t) \sum_{l=0}^{l=f-1} [a_l \cos(\omega_l t) + b_l \sin(\omega_l t)]. \quad (15)$$

The (angular) frequencies $\omega_l = \omega_0 + l\Delta\omega$ are equally spaced (by $\Delta\omega$) in an interval symmetric around a central frequency which dominates the pulse. The coefficients a_l and b_l can initially be chosen to be random numbers (with restrictions, e.g., fulfilling a certain norm). Further $s(t)$ is again a shape function, making the pulses "smooth" in particular at the beginning and end of the pulse (similar to the penalty function $\alpha(t)$ in OCT).

The basic idea of the SPO algorithm is to repeatedly use a population of laser pulses in the propagations, calculate a *fitness*, F, for each pulse (which depends on the purpose/target of control), and to find the optimal pulse by repeated stochastic variation of the expansion coefficients of the pulses. The optimization starts with a set of pulses, randomly generated (with restrictions). For these pulses an initial propagation is carried out and the fitness calculated. Expansion coefficients for a new generation of children are generated from the first (now parent) generation by mutation, at a mutation rate, M. Afterward, time-dependent simulations are carried out for all children and their fitness determined. A new generation of parents is selected from the family (parents and children) according to their fitness. From these new parents children are generated and the process starts again. This is done for a certain number of generations. The pulse with the highest fitness in the last generation, is the best pulse obtained for the given purpose. Details of the procedure can be found in Ref. 17. A specific example will be shown later.

5.3 Treatment of ionization

At larger laser intensities, on the order of 10^{13} W/cm^2 and beyond, ionization losses due to multiphoton excitations cannot be neglected. Ionization could be and has been treated, by using large grid bases. Using direct-product grids for correlated, wavefunction (rather than DFT) based N-electron dynamics in real, chemically relevant molecules is prohibitive, however. In this work we apply and compare two different, approximate models to treat ionization in molecules instead, using atomic orbital (AO) like basis sets.

5.3.1 A heuristic ionization model

In the first model, we include ionization within the TD-CIS/AO scheme, by augmenting the CIS energies with an imaginary part[46]:

$$E_n^{\mathrm{CIS}} \rightarrow E_n^{\mathrm{CIS}} - \frac{i\hbar}{2}\Gamma_n. \tag{16}$$

Here, Γ_n is a heuristically chosen ionization rate out of CIS state n, given as[46]

$$\Gamma_n = \begin{cases} 0 & \text{if} \quad E_n^{\mathrm{CIS}} < \mathrm{IP} \\ \displaystyle\sum_a \sum_r \left|D_{a,n}^r\right|^2 \frac{\sqrt{2\varepsilon_r}}{d} & \text{if} \quad E_n^{\mathrm{CIS}} \geq \mathrm{IP} \quad \text{and} \quad \varepsilon_r > 0. \end{cases} \tag{17}$$

That is, only CIS states above the ionization potential (IP) are assigned a finite ionization rate. The decay rate of CIS state n above IP, is given by a sum of classical, ballistic escape rates ($\sqrt{2\varepsilon_r}/d$) of an electron from virtual orbital r with energy ε_r, weighted by the probability $|D_{a,n}^r|^2$ that orbital r has been populated from an occupied orbital a. Note that d in Eq. (17) is an "escape" length after which the electron can be considered free, i.e., the molecule ionized. d is treated as a parameter below, with a final choice based on physical reasoning. Further, we calculate IP in the spirit of Koopmans' theorem, as $\mathrm{IP} = -\varepsilon_{\mathrm{HOMO}}$, where HOMO denotes the highest occupied MO in the HF ground state.

The heuristic ionization model has been used by several groups, e.g., Refs. 15–17,47. It was also tested against exact grid methods for few-electron systems,[48] and an "ab initio derivation" of the model was recently given in Ref. 49. In that reference, in addition an extension of the model to TD-CISD (i.e., including double excitations) was proposed.

5.3.2 An ionization model based on real-space absorbing potentials

An alternative way to treat ionization within TD-CIS/AO is to use complex absorbing potentials (CAPs) in real space. This idea has been realized by Schlegel and coworkers in Refs. 48, 50, and will occasionally be used in the following also. In the resulting *TD-CIS/CAP method*, the electronic Hamiltonian in Eq. (4) is extended by an imaginary absorbing potential,

$$\hat{H}(t) = \hat{H}_0 - \underline{\hat{\mu}}\underline{F}(t) - i\hat{V}^{\mathrm{CAP}}. \tag{18}$$

The role of the CAP is to impose outgoing boundary conditions to electrons reaching the continuum. For molecules, the absorber is taken as a sum of overlapping, atom-centered absorbers,

$$\hat{V}^{\mathrm{CAP}}(\underline{r}) = \sum_{A=1}^{N_A} V_A^{\mathrm{CAP}}(\underline{r} - \underline{R}_A). \tag{19}$$

Similar to previous work,[48,50] for the atomic contributions $V_A^{\mathrm{CAP}}(\underline{r} - \underline{R}_A)$ here we adopt spherical functions which are zero up to a distance R_A^0 from nucleus A, then increasing smoothly up to a maximum value V_{max}^{CAP}, from where on they stay constant. The precise form and parameters used for the V_A^{CAP} are described, for example, in Appendix A of Ref. 37. We also note that in the CAP approach, usually additional, diffuse AO basis functions are used as an "absorbing basis," to allow for sufficient overlap with the CAP region.[48,50,51]

5.4 Treatment of dissipation

Related to Sections 5.3.1 and 5.3.2, we note that electron dynamics based on TD-CI can also generally be extended to *open* quantum systems, in order to account for energy relaxation (of excited states) or dephasing (between different electronic states).[52,53] Examples where these effects play a role are spontaneous emission from excited states, ultrafast relaxation of excited molecules near metal surfaces,[52] or Auger (and other) decay of core-excited molecules.[54] In order to describe such effects with *norm-conserving* methods (in contrast to the energy- and real-space absorbers of above), we resort to reduced, Markovian, open-system density matrix theory by solving a Liouville-von Neumann equation,

$$\frac{\partial \hat{\rho}}{\partial t} = -\frac{i}{\hbar}\left[\hat{H}_0 - \hat{\underline{\mu}}\underline{F}(t), \hat{\rho}\right] + \mathcal{L}_D\hat{\rho}, \tag{20}$$

instead of the time-dependent electronic Schrödinger equation. Here, $\hat{\rho} = |\Psi(t)\rangle\langle\Psi(t)|$ is the electronic density operator. Within the so-called ρ-TD-CI method,[52] the connection to TD-CIS, for example, is made by expressing $\hat{\rho}$ in the basis of the CIS eigenstates Ψ_n^{CIS}. Then, diagonal elements ρ_{nn} give the population of CIS state $|n\rangle$, and ρ_{nm} ($n \neq m$) are coherences between different states.

There are various possibilities to choose the *dissipative* Liouvillian $\mathcal{L}_D$, which accounts for energy relaxation and dephasing, for example. In our own work, we usually used the *Lindblad* approach which is norm-conserving and completely positive by construction, reading

$$\mathcal{L}_D\hat{\rho} = \sum_n \left(\hat{C}_n\hat{\rho}\hat{C}_n^\dagger - 1/2\left[\hat{C}_n^\dagger\hat{C}_n, \hat{\rho}\right]_+\right). \tag{21}$$

Here, the $\hat{C}_n$ are Lindblad operators.[55,56] When energy relaxation by, e.g., spontaneous emission from (CIS) state $|k\rangle$ to state $|l\rangle$ is to be modeled, a convenient choice is

$$\hat{C}_n \rightarrow \hat{C}_{kl} = \sqrt{\Gamma_{k\rightarrow l}}|l\rangle\langle k| \tag{22}$$

with $\Gamma_{k\rightarrow l}$ being the transition rate. In case of spontaneous emission like processes these rates are given by

$$\Gamma_{k\rightarrow l} = A\,\mu_{kl}^2\,\omega_{kl}^3 \tag{23}$$

where μ_{kl} is the transition dipole moment connecting both states and $\hbar\omega_{kl} = E_k^{\mathrm{CIS}} - E_l^{\mathrm{CIS}}$ (in the CIS case). A is a constant which is $4/(3c^2)$ for spontaneous emission in vacuum, or an empirical value larger than that if an electron-rich environment, e.g., a metal surface is to be modeled instead.[52,57] Recently, a very similar formalism with empirical decay rates has been used to model electron dynamics including ultrafast Auger decay of core-excited molecules.[54] Further, the Lindblad/CIS and Lindblad/CIS(D) approaches were also used to account for *pure* dephasing,[52,57,58] and for dissipative processes in ionizing systems.[53,59] In the latter case, the Hamiltonian part of the total Liouvillian is complemented by a term $-\frac{i\hbar}{2}\sum_n \Gamma_n |n\rangle\langle n|$ within the "heuristic" ionization model introduced above.

6. Electronic wavepackets

6.1 Uncorrelated vs correlated electron dynamics: LiH

As a first example, which also illustrates one of the methodological aspects of above, let us consider a LiH molecule, driven by an ultrashort, 3-cycle, $\cos^2$-shaped laser pulse of the form given by Eqs. (9) and (10). In the specific example, the laser is polarized along the molecular axis (z, say), the pulse has a full width of $2\sigma = 124\ \hbar/\mathrm{E}_h$ (3 fs), at a carrier frequency of $\omega_0 = 0.15\ \mathrm{E}_h/\hbar$ ($1\ \mathrm{E}_h = 1$ Hartree), corresponding to $\hbar\omega_0 = 4.1$ eV. This is close to several excited states of the LiH molecule.[60,61] The carrier envelope phase was chosen as $\phi_{\mathrm{CEP}} = 0$. The maximum field strength F_0 will be specified shortly.

We are not interested in detail here in the physics of the excitation event nor its dependence on the exciting laser pulse, which has extensively been described elsewhere.[61] Rather, we focus on a comparison of "uncorrelated" electron dynamics with "correlated" electron dynamics. The latter is

captured by an MCTDHF calculation in the form of TD-CASSCF(4,4) (i.e., all four electrons in four spatial orbitals), the latter by a TD-HF, or TD-CASSCF(4,2) calculation, in the nomenclature introduced earlier. In both cases, a rather extended, AO-like (Gaussian) basis set (6-311++G (2df,2p)) is used.[61] As initial state for the propagation, the ground state within the respective method (RHF *vs* CASSCF(4,4)) was taken, and the Li-H distance was fixed at a value of 3.08 a_0.

We consider first in Fig. 1A the case of a moderate field amplitude of $F_0 = 0.01$ $E_h/(ea_0)$ (e = elementary charge, a_0 the Bohr radius), corresponding to a peak intensity of 3.5×10^{12} W/cm^2. As can be seen from Fig. 1A, upper panel, for both methods, correlated and uncorrelated, the energy expectation value $\langle \Psi(t)|\hat{H}_0 - \underline{\hat{\mu}}\underline{F}(t)|\Psi(t)\rangle$ changes in response to the 3-cycle laser pulse. After the pulse is off, the energy remains constant at an elevated energy (the energy gain is 0.0185 E_h (0.5 eV) in the case of TD-CASSCF(4,4)), due to the formation of an electronic wavepacket by partial occupation of higher excited states. While the energy remains constant after the pulse, this is not the case for other properties such as the molecular

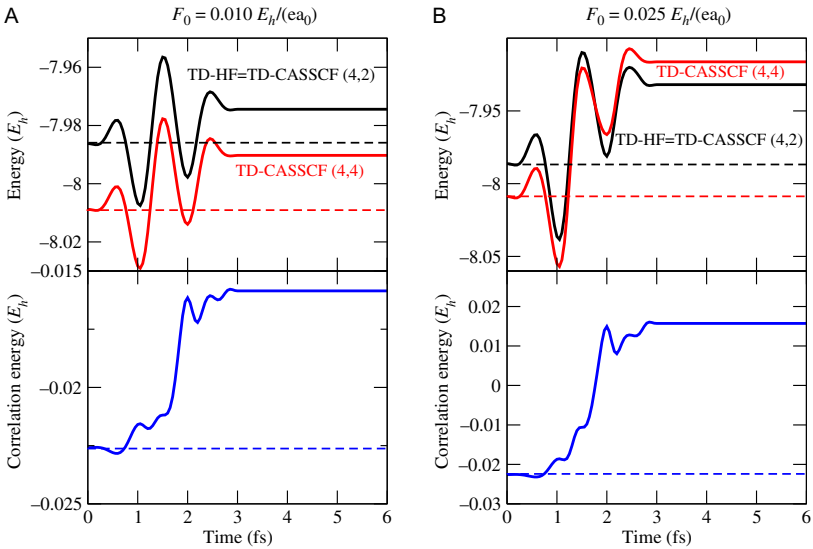

Fig. 1 LiH molecule interacting with two cos^2-shaped, 3-fs, 3-cycle laser pulses of different intensity (see text) with $\hbar\omega_0 = 0.15$ E_h. The upper panels show energy expectation values obtained with TD-HF/6-311++G(2df,2p) (or TD-CASSCF(4,2)) and TD-CASSCF (4,4)/6-311++G(2df,2p) methods, the lower panels the energy difference $E_{\text{TD-CASSCF}} - E_{\text{TD-HF}}$, somewhat sloppy denoted as "correlation energy." (A) $F_0 = 0.010$ $E_h/(ea_0)$; (B) $F_0 = 0.025$ $E_h/(ea_0)$.

dipole moment, which keeps oscillating in time since a wavepacket is formed[61] (not shown here). Note that for energies at least, the behavior of TD-CASSCF(4,4) and TD-HF is similar as far as the overall shape of the energy curves is concerned: both curves run more or less parallel. Closer inspection shows that the energy difference $E_{\text{TD-CASSCF}} - E_{\text{TD-HF}}$, which is denoted as "correlation energy" in the figure, changes slightly with time. We emphasize that the notion of "correlation energy," borrowed from stationary quantum chemistry, is valid only for $t = 0$, before the pulse, and should strictly not be used thereafter.

The situation changes quite a bit if another, larger field strength is considered, $F_0 = 0.025$ $E_h/(ea_0)$, corresponding to an intensity of 2.2×10^{13} W/cm^2 (Fig. 1B). Then, in the TD-CASSCF case now much more energy is gained than for TD-HF—in fact the TD-CASSCF energy is *larger* after the pulse than the TD-HF energy, despite initially, before the pulse, the HF energy is of course lower than the CASSCF(4,4) energy. From the lower panel of Fig. 1B we see that the formal "correlation energy" would then be even positive after the pulse, which shows that the usual definition of correlation energy makes no sense in a time-dependent context and/or when a laser pulse is applied. In general, however, this simple example of laser-driven LiH may already serve to illustrate the importance of correlation, also in electron dynamics.

6.2 Building up electron correlation: An attosecond process

A Hartree-Fock ground state Slater determinant is not an eigenfunction of the field-free electronic Hamiltonian as defined in Eq. (5). From the point of view of electron dynamics, in fact, the HF ground state is a *wavepacket* instead, i.e., its time-evolution under the influence of the full, field-free Hamiltonian is

$$\Psi(t) = e^{-i\hat{H}_0 t/\hbar}\, \Psi_0^{\text{HF}} = \sum_n C_n\, e^{-iE_n t/\hbar}\, \Psi_n, \tag{24}$$

where the Ψ_n are now the (correlated) eigenfunctions of $\hat{H}_0$ with energies E_n. The C_n, now time-independent, are obtained from projection of Ψ_0^{HF} on Ψ_n, i.e., $C_n = \langle \Psi_n | \Psi_0^{\text{HF}} \rangle$. If the correlated eigenstates are represented/approximated by CI states, then, for CISD, for example, Ψ_n and E_n in Eq. (24) become Ψ_n^{CISD} and E_n^{CISD}, respectively.

In Fig. 2A, we illustrate the wavepacket dynamics of the initial HF ground state of a H_2 molecule, $\Psi(t = 0) = \Psi_0^{\text{HF}}$ at its optimized geometry

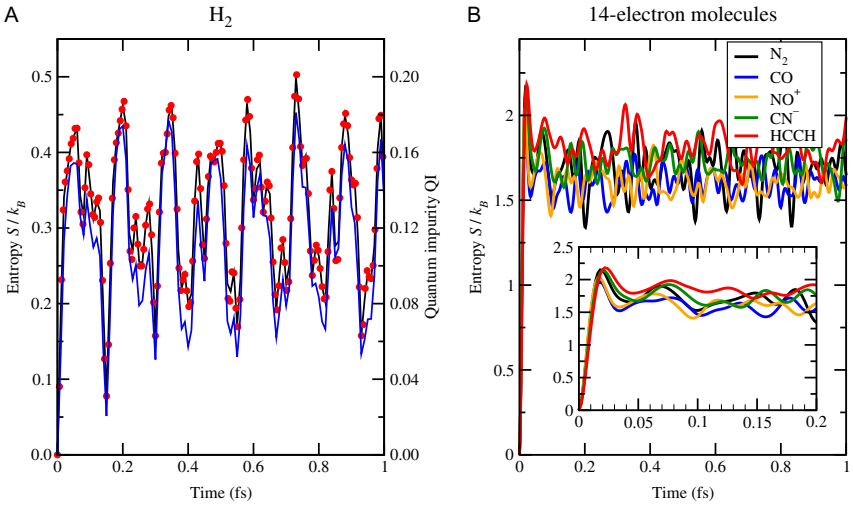

Fig. 2 (A) Correlation measures $S(t)$ (left scale, *black curve*) and $QI(t)$ (right scale, *blue curve*) of a H_2 molecule, when applying the exact, field-free electronic propagator $e^{-i\hat{H}_0 t/\hbar}$ to a RHF ground state, using TD-CISD/6-31G*. The *red dots* show $S(t)$ obtained with TD-CASSCF(2,10)/6-31G*.[63] (B) Entropy $S(t)$ of various 14-electron molecules, when applying the exact, field-free electronic propagator to the RHF ground state, using TD-CISD/6-31G*. The *inset* enlarges the short-time behavior. See text for further details. (A) H_2; (B) 14-electron molecules.

(at the RHF/6-31G* level of theory), when the "exact" electronic propagator $e^{-i\hat{H}_0 t/\hbar}$ is applied, using the TD-CISD/6-31G* method. The two solid curves shown there correspond to two different, time-dependent measures of electron correlation, much more suitable as the "correlation energy" of above, namely, the *entropy*, S, and a quantity which we call "*quantum impurity*," QI.[62] The former is calculated as a trace

$$S = -k_B \mathrm{Tr}(\rho_1 \ln \rho_1) \tag{25}$$

where ρ_1 denotes the reduced one-electron density matrix (1RDM), defined as

$$\rho_1(\underline{x}; \underline{x}'; t) = N \int \Psi(\underline{x}, \underline{x}_2, \ldots, \underline{x}_N; t) \Psi^*(\underline{x}', \underline{x}_2, \ldots, \underline{x}_N; t)\, d\underline{x}_2 \ldots, d\underline{x}_N \tag{26}$$

where $\underline{x}_i = (\underline{r}_i, s_i)$ is the combined position-spin variable of electron i, and $\Psi(t)$ is an N-electron wavefunction. An uncorrelated situation arises, if the many-electron system is described by a single determinant. We express the

1RDM in the basis of Hartree-Fock orbitals χ_k, i.e., as a matrix $\underline{\underline{\gamma}}$ with elements

$$\gamma_{ij} = \int d\underline{x}\; d\underline{x}'\; \chi_i^*(\underline{x})\; \rho_1(\underline{x},\underline{x}')\; \chi_j(\underline{x}'). \tag{27}$$

Further, the quantum impurity is calculated as

$$QI(t) = 1 - \mathrm{Tr}\{\rho_1(t)^2\}/N. \tag{28}$$

Note that both S and QI start from 0 (the uncorrelated HF state), then increase to higher level ($\sim 0.25\ k_B$ for the entropy), and start to oscillate at an elevated, average value ($\sim 0.4\ k_B$ for the entropy). The oscillation period is inversely proportional to the energy differences between correlated (in our case CISD) states of the molecule as argued in Ref. 62. The initial rise of the two curves to the first maximum, at $t \sim 50$ as, can be interpreted as the "onset time"/"reappearance" of electron correlation, i.e., the time needed for the two electrons in H_2 to correlate with each other. In Fig. 2A we show also entropies obtained with the TD-CASSCF(2,10)/6-31G* method (red dots), which nicely agree with the TD-CISD results.

The onset/reappearance of electron correlation on the timescale of a few tens of attoseconds is, for molecules, a rather generic feature. This is demonstrated in Fig. 2B, where we show similar curves for series of molecules with 14 electrons. Again, the TD-CISD/6-31G* method was used to propagate HF initial states (at RHF/6-31G* geometries). Also there, an initial rise of the entropy occurs (within 20 as or so), followed by oscillations around an elevated value of S. We may coin the ultrafast phenomenon of correlation buildup in molecules as "correlation-driven electron dynamics." This nomenclature is in analogy to a similar phenomenon predicted theoretically by Cederbaum and coworkers,[64] which was recently verified experimentally[65,66]: the *charge migration* in molecules after sudden ionization. Charge migration is also ultrafast (much faster than nuclear motion), proceeding typically on the timescale of a few tens of attoseconds. We finally note that similar timescales for the reappearance of correlation have also been predicted for other molecules, and also for atoms, in Ref. 62.

6.3 Toward creating a Hartree-Fock state by laser pulse excitation

In Ref. 62, it was also suggested, how to possibly *create a Hartree-Fock state*, i.e., an electronic wavepacket, from a correlated ground state. The key to do

so was to apply optimal control theory of above, where the target operator defined in Eq. (12) was constructed from the desired HF state, i.e.,

$$\hat{O} = |\Psi_0^{\mathrm{HF}}\rangle\langle\Psi_0^{\mathrm{HF}}|, \tag{29}$$

or an approximation thereof. In Ref. 62, this was done for atoms mostly. Here we show in Fig. 3 a molecular example instead,[63] namely the creation of a HF state (or an approximation to it) for H_2. The H_2 molecule is aligned along the z-axis and a bond length of 0.74 a_0 is considered. We start at the (correlated) CISD ground state, $\Psi(0) = \Psi_0^{\mathrm{CISD}}$, obtained with Dunning's cc-pVQZ basis. We then run TD-CISD/cc-pVQZ/OCT calculations, in which independently the two components of a laser pulse polarized perpendicular to the molecular axis are optimized, i.e., we optimize the F_x and F_y components of the pulse $\underline{F} = (F_x(t), F_y(t), 0)$. The control time

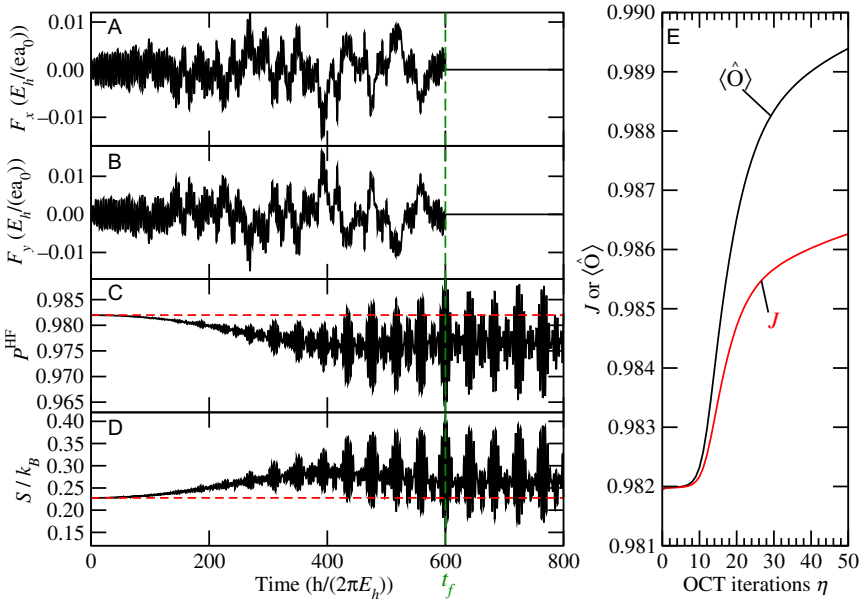

Fig. 3 Illustration of the application of OCT to create a HF state of H_2, from a correlated ground state, Ψ_0^{CISD}.[63] Figs. (A) and (B) show the field components $F_x(t)$ and $F_y(t)$ for a chosen control time $t_f = 600\ \hbar/E_h$ (*vertical green*, *dashed line*), obtained after 50 OCT cycles. (Note: 600 $\hbar/E_h$ are 14.5 fs.) Figs. (C) and (D) give the HF state contributions P^{HF} and entropy S as a function of time, with elevated P^{HF} and reduced S, at $t = t_f$. The initial values are shown as *dashed, red lines*. (E) Expectation value of the target operator $\hat{O}$ (in other words, $\langle\hat{O}\rangle = \langle\Psi(t)|\hat{O}|\Psi(t)\rangle = P^{\mathrm{HF}}$), and of the functional J in Eq. (11) as a function of the number of iterations within the OCT cycle. All calculations were done on the (TD-)CISD/cc-pVQZ level of theory. See text for further details.

(pulse length) t_f was chosen as 600 $\hbar/\mathrm{E}_h$ (ca. 14.5 fs). In the target operator (29), Ψ_0^{HF} is a wavepacket comprising 1830 CISD eigenstates obtained with the chosen basis. 50 iterations of the OCT algorithm were run, with a penalty function in Eq. (11) chosen as $\alpha(t) = \alpha/g(t)$, where $\alpha = 0.15$ and $g(t) = \exp\left(-\left((t - t_f/2)/t_f\right)^{12}\right)$. The initial pulse is generated with random field components along x and y.

Fig. 3C shows the portion of the HF-character contained in the time-dependent wavefunction $\Psi(t)$, measured by

$$P^{\mathrm{HF}}(t) = |\langle\Psi(t)|\Psi_0^{\mathrm{HF}}\rangle|^2 = \langle\Psi(t)|\hat{O}|\Psi(t)\rangle. \tag{30}$$

Note that at $t = 0$ (when $\Psi(t) = \Psi_0^{\mathrm{CISD}}$), $P^{\mathrm{HF}}(0) = 0.982$, corresponding to a one-electron entropy $S(0)$ of around 0.0228 k_B according to Fig. 3D. After applying the OCT algorithm for 50 cycles, at the end of the pulse, we achieve $P^{\mathrm{HF}}(t_f) = 0.9895$, and $S(t_f) = 0.0153$. Thus, the wavefunction was forced closer to the HF state (indicated by $P^{\mathrm{HF}}(t_f)$ closer to 1 and $S(t_f)$ closer to 0), but it is also seen that the HF state was not fully reached yet after 50 OCT iterations. This is also demonstrated in Fig. 3E, showing $P^{\mathrm{HF}}(t_f)$ as a function of OCT iterations, η. We further note that outside the target time (t_f), the target values (large P^{HF} and small S) may even be worse than for the initial correlated state. In particular, after the pulse is off, high-frequency oscillations (in P^{HF} and S) are observed similar to those of Fig. 2A. We finally note that the optimal control pulse, after 50 iterations, is quite complicated (cf. Fig. 3A and B). Maximal field strengths are around $|F_i| \sim 0.01 - 0.015\ \mathrm{E}_h/(\mathrm{ea}_0)$, both for $i = x$ and y, corresponding to a (total) intensity of around 10^{13} W/cm^2.

In summary, the OCT algorithm with 50 iterations brought us closer to a HF state, and correlation was diminished. In Ref. 62 for certain atoms such as Mg or Be, pulses were theoretically designed which gave P^{HF} values even closer to 1 and entropies very close to 0, at least under certain physical simplifications made there (linearly polarized laser pulses, neglect of ionization losses, up to double excitations only). It remains to be seen if an experiment could be made working, in which such pulses are designed in practice. If so, a so far purely theoretical but extremely important concept of quantum chemistry, namely the Hartree-Fock state, might be brought to real existence. Since this is a wavepacket coming with oscillating properties, e.g., oscillating molecular dipole moments, a possible way to detect it could be emitted radiation. For an oscillation period τ in the order of 50 as

(cf. Fig. 2B), one expects an emission frequency of $\omega = 2\pi/\tau \sim 3\ E_h/\hbar$ (corresponding to $\hbar\omega \sim 80$ eV), or a wavelength of around 15 nm—which is in the VUV regime.

7. High harmonic generation

7.1 HHG spectra for molecules: Models and computation

As stated above, good progress has been made in creating, interpreting, and modeling HHG radiation in *molecules* in recent years. HHG is usually rationalized by Corkum's semiclassical three-step model.[67] Accordingly, a single electron, created by tunnel ionization is first accelerated away from the parent ion in the laser field, then after field sign reversal driven back to the mother ion, where finally, inelastic recollision causes emission of photons with frequencies at integer multiples of the driving frequency, ω_0 (which should *not* be resonant with a state-to-state transition in this case). By the driving field, a wavepacket is created which gives rise to a time-dependent (induced) dipole moment, which is related to the HHG signal (see below). Corkum's model nicely explains the "typical" shape of a HHG spectrum, namely (i) an initial rapid falloff of the intensity of the lowest harmonics, (ii) followed by a "plateau region" (with rather constant HH intensities), and (iii) a rapid decline of the signal intensities beyond a cutoff frequency $\omega_{\max}$, which depends on the laser parameters and the ionization potential of the emitting system. Beyond this semiclassical, single-active electron model, quantum effects,[68] multielectron effects,[8,9] and characteristic interference effects[7,9,69] come into play, which can modify the simple picture, causing, e.g., intensity dips in HHG spectra.[9] Further, HHG also depends sensitively on symmetry, e.g., in aligned molecules with inversion symmetry only odd harmonics are seen.

In what follows we do not use the semiclassical three-step model, but compute HHG spectra for molecules by solving the electronic TDSE instead. All HHG spectra in this paper are computed for linearly polarized pulses as follows. In the aligned/single polarization case, we calculate HHG intensities for laser polarization i, by

$$I_i(\omega) = A\left|\int_0^{t_f} \beta_i(t)\ w(t)\ e^{-i\omega t} dt\right|^2 . \tag{31}$$

In Eq. (31), $w(t)$ is a window function, which can be used to improve the signal-to-noise ratio, and t_f is the final time considered. There are three

formally equivalent and in practice almost equivalent ways[70] of how to choose $\beta_i(t)$ (and the prefactor A) to calculate HHG spectra. In the *dipole length form*, we take β_i as the projection of the time-dependent dipole moment vector $\underline{\mu}_i(t)$ on the polarization (unit) vector:

$$\beta_i(t) = \mu_i(t) = \underline{\mu}_i(t)\underline{P}_i. \tag{32}$$

In the *dipole velocity form*, we take

$$\beta_i(t) = \frac{d\mu_i(t)}{dt} \tag{33}$$

and in the *dipole acceleration form*, we take

$$\beta_i(t) = \frac{d^2\mu_i(t)}{dt^2}. \tag{34}$$

In fact, $\omega^2 I_\mu(\omega) \sim I_\nu(\omega) \sim I_a(\omega)/\omega^2$ in practical calculations,[70] where I_μ, I_ν and I_a are notations for the HHG signal obtained with integrals done in the dipole length (μ), dipole velocity (ν), and dipole acceleration forms (a), respectively. The prefactor A in Eq. (31) is chosen "arbitrarily" as specified below—in particular a possible ω-dependence is neglected. Note that, when using absorbing boundaries, we do not renormalize the electronic wavefunction when computing the dipole moment, to account for possible ionization losses.

In some cases, for unaligned molecules, a coherently, rotationally averaged HHG spectrum for a given set of M polarization vectors will be computed, by first defining a total, averaged (induced) dipole moment (cf. Eq. 32)

$$\overline{\mu}(t) = \frac{1}{M}\sum_{i=1}^{M}\mu_i(t). \tag{35}$$

From there we calculate averaged functions $\overline{\beta}(t)$ and then coherently, rotationally averaged HHG intensities $\overline{I}(\omega)$, by replacing $\beta_i(t)$ by $\overline{\beta}(t)$ in the integral in Eq. (31).

7.2 A first example: H_2

As a first example, we consider once more the H_2 molecule for pedagogical reasons, at an interatomic distance of 1.4 a_0 (0.741 Å). The molecule is excited by a laser pulse of the form (9,10), linearly polarized along the molecular axis, with the following parameters: $\hbar\omega_0 = 0.057$ E_h (1.55 eV, corresponding to 800 nm), $2\sigma = 2205$ $\hbar/E_h$ (or 53.3 fs, corresponding to 20 optical cycles),

$t_p = \sigma$, $\phi_{\mathrm{CEP}} = 0$ and an intensity of 1×10^{14} W/cm^2, corresponding to a field amplitude of 0.053 $E_h/(ea_0)$. The HHG signals shown in Fig. 4A were calculated from Eq. (31) in the dipole length form (setting $A = 1/t_f$, $t_f = 2\sigma$ and choosing a Hann window function for $w(t)$), with an induced dipole moment obtained from TD-CIS/aug-cc-pVDZ, starting initially from the RHF/aug-cc-pVDZ ground state.

The two curves shown in Fig. 4A refer to the situation when no ionization losses have been modeled (black curve, "no lifetimes"), and to a case where ionization losses have been considered by using the heuristic lifetime/ionization model of Eq. (17) with the choice $d = 1$ a_0 (red curve, "with lifetimes"). Both curves reflect the rather "generic" form of the HHG spectra with a fast initial signal drop, a plateau, and a cutoff region. According to Corkum's semi-classical 3-step model, the cutoff number (highest harmonic emitted) is

$$N_{\mathrm{cut}} = \left(\mathrm{IP} + 3.17\frac{F_0^2}{4\omega_0^2}\right)/(\hbar\omega_0) \tag{36}$$

which gives with the present laser parameters and the choice IP = 15.4 eV from experiment, $N_{\mathrm{cut}} \sim (15.4 + 3.17 \times 6.0)/1.55 \sim 22$. This agrees roughly also with the results of the TD-CIS calculations. Note, however, that only odd harmonics are seen in the aligned/single-polarization case, due to the inversion symmetry of H_2. We also observe that ionization obviously plays a role: The spectrum without ionization is more noisy and more intense than the one with ionization losses, due to artificial reflections of the wavepacket far from the molecular center when finite AO basis sets are used. In fact, the convergence of HHG spectra with Gaussian/AO basis set size, particularly for the higher harmonics, is a delicate issue.[16,70] The use of diffuse and high-angular momenta functions (e.g., so-called Kaufmann functions[70]) captures the large-amplitude motion of electrons better, and also not atom-centered basis functions are beneficial.[17,37,70] Using absorbing boundaries (here in energy space) is a practical, approximate way to mimic the effect of more extended basis sets and/or grids and/or B-splines,[71] which would allow for more realistic behavior of electron wavepackets created by intense laser pulses, namely large-amplitude motions and ionization. In the present example, the ionization loss is around 30 % (not shown).

One may also ask if it is possible, apart from simply controlling the cutoff of HHG spectra by changing the laser parameters F_0 and ω_0 in Eq. (36), to *control* the nonlinear, HHG response of molecules by laser pulse design.

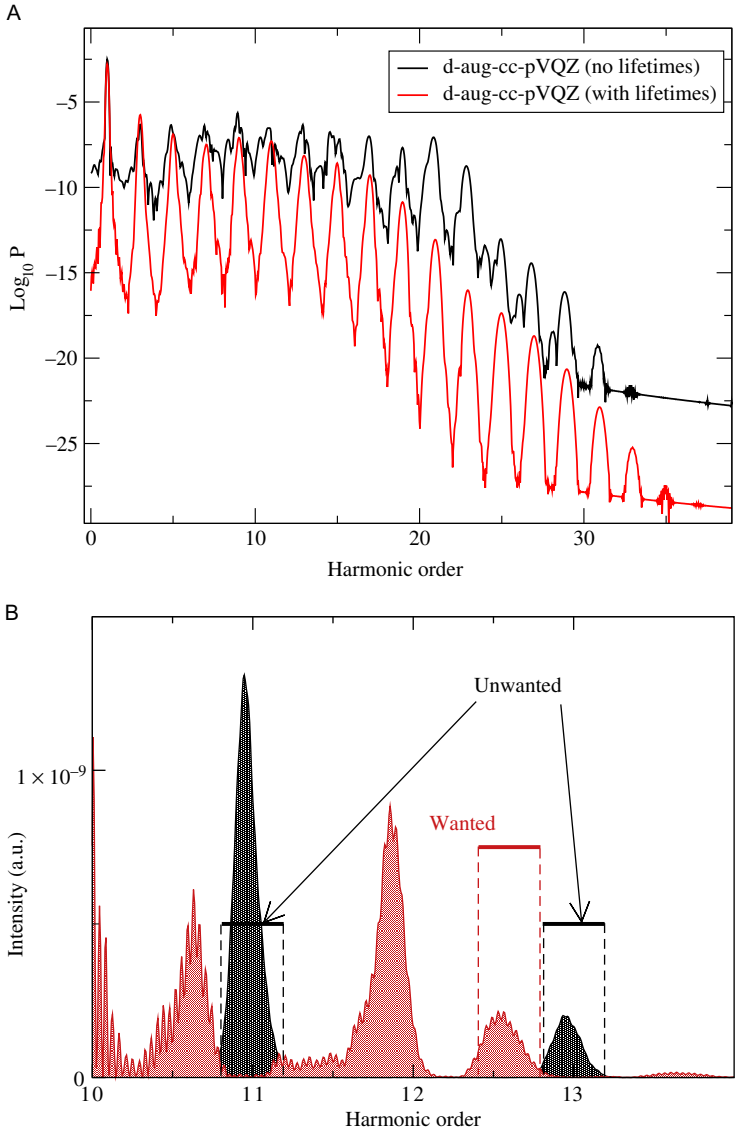

Fig. 4 HHG spectra for H_2 and their control. In (A) we show HHG spectra (calculated in the dipole length form) of H_2 when driven by a 20-cycle ($2\sigma = 2205\ \hbar/E_h$) $\cos^2$-pulse with a field amplitude $F_0 = 0.053\ E_h/(ea_0)$, wavelength = 800 nm. Calculations were done on the TD-CIS/d-aug-cc-pVQZ level of theory with and without the inclusion of lifetime effects[16] (see text). (B) Control of HHG spectra of H_2, by using the stochastic pulse optimization (SPO) scheme.[17] The *black curve* shows two harmonics (11 and 13, scaled by a factor of 10) in the "cutoff region," for a $\cos^2$-pulse with $\lambda = 800$ nm, $2\sigma = 2000\ \hbar/E_h$ and $F_0 = 0.0125\ E_h/(ea_0)$, obtained with TD-CIS/aug-cc-pVQZ and by using the dipole acceleration form (see text for further details). The red curve shows the HHG spectrum in this region after the application of the SPO algorithm. "Wanted" and "unwanted" regions are indicated by *horizontal bars* and *vertical lines*.

An example would be to either suppress "unwanted" harmonics, and/or to increase HHG intensities in predetermined frequency ranges. There have been several attempts in these directions, both experimentally[72–74] and theoretically. Considering the latter, Balogh et al.[75] used a genetic algorithm to optimize the individual width and the spacing between the pulses of an attosecond pulse train in a modeled experimental setup. Further, Castro et al.[76] showed that by use of optimal control theory, it is possible to selectively enhance specific harmonics by shaping the envelope of a 800 nm carrier laser pulse.

In our own work,[17] we have used the stochastic pulse optimization scheme described above to control HHG responses of molecules, an example of which is shown in Fig. 4B. There, again H_2 was considered ($R_{H\text{-}H} = 1.4\ a_0$), and TD-CIS/cc-pVQZ calculations including ionization losses via the heuristic ionization model of above were carried out for pulses linearly polarized along the molecular axis (z). HHG signals were calculated in the dipole acceleration form from Eqs. (31) and (34) (with $A = 1/\sqrt{2\pi}$, $w(t) = 1$). In a first example, a $\cos^2$-shaped pulse was used, again with $\hbar\omega_0 = 1.55\,\text{eV}$ (corresponding to $\lambda = 800$ nm) and $\phi_{CEP} = 0$, but now with $2\sigma = 2000\ \hbar/E_h$ (slightly different from Fig. 4A), and $F_0 = 0.0125\ E_h/(ea_0)$ (corresponding to $5.5 \times 10^{12}\ \text{W/cm}^2$). As a consequence of the lower intensity, the Corkum cutoff (36) is now shifted down to $N_{cut} \sim 11$. The black curve in Fig. 4B shows the HHG spectrum in a small region around the expected cutoff, exhibiting two clear signals at the odd harmonics 11 and 13. (Lower harmonics are typically higher in intensity as expected, cf. Ref. 17.) A goal formulated in Ref. 17 was to suppress the two signals 11 and 13 as much as possible (unwanted frequency regions), while at the same time enhancing the signal intensity in a narrow frequency region around $\omega = 12.6\ \omega_0$ ("wanted" frequency region). This was attempted by using a fitness function in the SPO algorithm, of

$$F = \frac{\sum_k W_k |\mu_z(\omega_k)|^2}{\sum_k U_k |\mu_z(\omega_k)|^2}. \tag{37}$$

Here, we sum over components of the power spectrum of the dipole moment for wanted frequencies weighted with corresponding, freely chosen weights (W_k), divided by an analogous expression for unwanted contributions (weights U_k). The power spectrum was calculated through a discrete Fourier transformation of $\mu_z(t)$, in the interval $[0, t_f]$, with t_f being the final propagation time. How the weights U_k and W_k were

chosen (essentially large W_k and small U_k), and further details can be found elsewhere.[17] By optimizing the laser pulse comprising 73 frequencies equally spaced in an interval between $\hbar\omega = 0.01696$ E_h (0.46 eV) and $\hbar\omega = 0.09696$ E_h (2.64 eV), after 200 iterations of the SPO algorithm one obtains the red curve in Fig. 4B. It is nicely seen that the first part of the goal, the complete suppression of the former $n = 11$ and $n = 13$ harmonic signals, was fully achieved. Also, some signal appears in the "wanted area," as desired. We do note, however, that also intensity appears in areas for which no special weighting factors were introduced, i.e., in the uncontrolled areas, e.g., around $n \sim 11.8$. It is expected, that by a proper modification of the fitness function (e.g., an extension of "unwanted areas"), the response also in these frequency regions can be controlled.

7.3 Larger molecules

7.3.1 The N_2O molecule

The TD-CIS/AO method is a very efficient method to calculate HHG spectra also for larger molecules. As said, a problem is, however, that higher harmonics are usually difficult to converge with Gaussian, atom-centered basis sets. On the other hand, for correlated WFT the use of extended grid bases is prohibitive for larger systems and molecules in three dimensions. Absorbing boundaries (in energy or real space) not only account for ionization losses, they also remove some of the artifacts of atom-centered basis sets, suppressing noisy structures in HHG spectra (see above).

Keeping the mentioned limitations of TD-CIS/AO methods in mind, let us consider the N_2O molecule, driven by $\cos^2$-shaped laser pulses according to Eqs. (9) and (10), with $\hbar\omega_0 = 0.0351$ E_h (1300 nm), being 20 optical cycles long (i.e., $2\sigma = 3577\ \hbar/E_h$ (86.5 fs)), $\phi_{CEP} = 0$. In Fig. 5A, computed HHG spectra for N_2O are shown, either for the "aligned" molecule driven by a laser polarized along the molecular axis (z), or a coherently, rotationally averaged spectrum, with averaging done over 162 polarization vectors with endpoints maximally uniformly distributed on the surface of a sphere as outlined above. In this case, the laser pulse intensity was fixed at $I = 10^{14}$ W/cm^2. All calculations were performed with the TD-CIS/aug-cc-pVQZ method, for linear N_2O, with $R_{N\text{-}N} = 1.082$ Å and $R_{N\text{-}O} = 1.169$ Å. Absorbing boundaries to account for ionization were included via the real-space CAP method described above. The total absorbing potential is constructed from a set of overlapping spherical potentials around each atom, Eq. (19), starting at a distance of five times

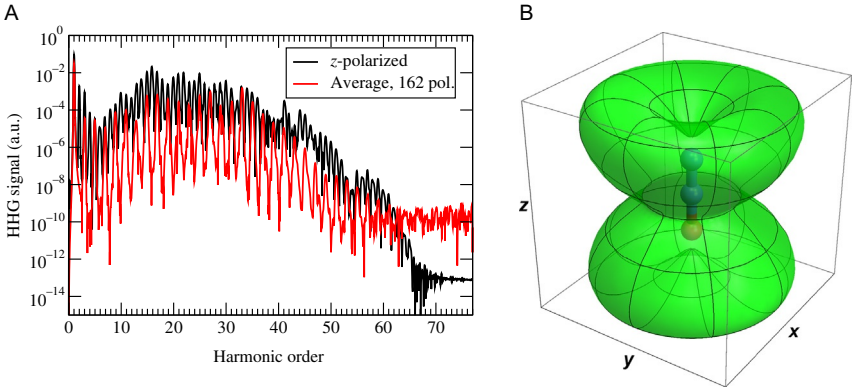

Fig. 5 (A) HHG spectra of N_2O obtained with TD-CIS/aug-cc-pVQZ/CAP, for an aligned molecule driven by a 1300 nm laser pulse (20 optical cycles long, $I = 10^{14}$ W/cm^2) polarized along the molecular axis (*z*), shown in *black*. The *red curve* gives a rotationally averaged spectrum, considering 162 polarization directions. In (B) we show for the same molecule and method, with a different laser pulse (800 nm, 7 optical cycles long, $I = 2.25 \times 10^{14}$ W/cm^2, considering 84 polarization directions) a surface surrounding the N_2O molecule, to quantify the angular dependence of ionization losses (see text).

the van der Waals radius of each element (at 17.291 a_0 for N and 16.5351 a_0 for O). The atomic absorbing potentials have a quadratic rise and a quadratic turn over to a constant value of 10 E_h at long-range. For the CAP calculations, extra basis functions at the O atom and at the outer N atom were added as an "absorbing basis" (six s functions (with even-tempered exponents from 0.0256 to 0.0008 atomic units), four p (even-tempered exponents from 0.0256 to 0.0016, except 0.0064), five d (even-tempered exponents from 0.0512 to 0.0016, except 0.0064), three f (even-tempered exponents from 0.0256 to 0.0064), one g and one h shell (each with an exponent of 0.0512). The HHG spectra were calculated within the dipole acceleration form from Eq. (31) (with $A = 1/\sqrt{2\pi}$, $w(t)$ being a Hann function, $t_f = 2204.7\ \hbar/E_h$).

From Fig. 5A, we first note HHG spectra with a slight "non-Corkum" behavior (e.g., intensity dips in some regions, qualitatively similar to experiment[9]). Still, cutoff regions can be recognized. For the laser parameters at hand, taking the Corkum expression (36) with the experimental ionization potential IP = 12.89 eV, we obtain $N_{\mathrm{cut}} \sim 66$, which is close to what we see in the calculations also. We further note that there are differences between "aligned" and "averaged" spectra. The most important difference is that in the latter case, in contrast to the former, only odd

harmonics are seen, even though the molecule has no inversion symmetry. This observation (which is in agreement with experimental findings) has to do with the fact that in the averaging process, even harmonics appearing at a single polarization are annihilated by a corresponding field vector in exactly opposite direction.

For intense laser intensities ionization losses can also not be neglected. Using pulses with even larger intensities than in Fig. 5A, ionization becomes substantial and will generally depend on the polarization of the incoming laser pulse. This is demonstrated in Fig. 5B, where we visualize ionization losses from N_2O when driven by laser pulses with 800 nm, seven optical cycles long, $I = 2.25 \times 10^{14}$ W/cm^2 along 84 directions (in this case by varying polarization angles θ and ϕ by 30°). The plot indicates the loss of norm of the electronic wavefunction along those directions: The length of a vector from the center of mass of the molecule to the green surface is proportional to the ionization loss in this direction, as detailed in Ref. 51. It is seen that these angle-dependent ionizations reflect the shape of the degenerated antibonding π highest occupied molecular orbitals of N_2O. Therefore, the loss is small in polarization directions along the molecular axis or exactly perpendicular to it, whereas polarization directions between these two extremes lead to larger ionization losses.

7.3.2 Isomers of organic molecules discriminated by HHG

As mentioned above, it has been suggested to discriminate between isomers of organic molecules by HHG spectroscopy.[10–12] Also here the TD-CIS/AO method proved to be an efficient and fairly accurate method that can help contribute to the theoretical understanding of the discrimination process from a many-electron dynamics perspective.[37] In Fig. 6, we show computed HHG spectra for cis- and trans-isomers of 1,2-dichloroethene (DCE), calculated either for fixed polarizations (parallel to the molecular plane), or when averaged over 162 orientations. In all cases, the TD-CIS/aug-cc-pVTZ-6-i method was used, where aug-cc-pVTZ-6-i refers to a special basis set including very diffuse functions as described in detail in Ref. 37. Further, the heuristic ionization model was used with parameters specified there also. If not stated otherwise, in accordance with experiment,[10] we choose laser pulses with a wavelength of 1800 nm, a peak intensity of 1.1×10^{14} W/cm^2, a pulse length $2\sigma = 160$ fs, and $\phi_{\mathrm{CEP}} = 0$ (cf. Eqs. (9) and (10)). HHG spectra were calculated in the dipole acceleration form, with further details given in Ref. 37. According to experiment[10] (see fig. 1 of that reference), for a laser with the same parameters as used in this work randomly

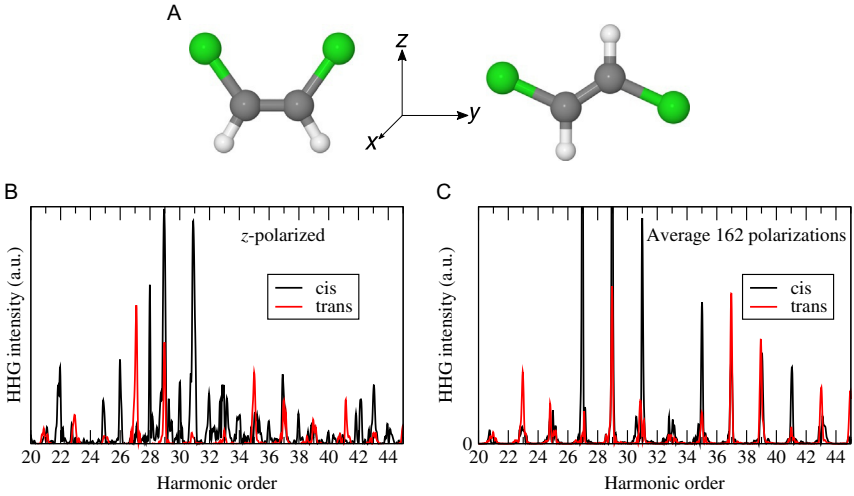

Fig. 6 Simulated HHG spectra of cis- and trans-DCE, computed on the TD-CIS/aug-cc-pVTZ-6-i level of theory, adopting the "heuristic ionization model."[37] The *upper panel* (A) shows the two molecular structures, computed with RHF/aug-cc-pVTZ, along with the coordinate system used. Panel (B) shows a portion of the HHG spectrum for cis- and trans-DCE, when generated with a 1800 nm laser pulse polarized in the molecular plane, along the *z*-direction. Intensities are given in arbitrary units, relative to harmonic 29 of cis, which is the most intense peak in the range shown. Panel (C) gives the corresponding HHG spectra, when averaged over 162 polarization directions. Intensities are given again in arbitrary units relative to harmonic 29 of cis, which is again the most intense signal in the shown range.

oriented cis-isomers exhibit clearly larger HHG intensities for harmonics 21–69 compared to the trans-isomers. As a second observation only odd harmonics were seen in experiment, both for cis and trans.

In Fig. 6 we show HHG spectra of cis- and trans-DCE (upper panel), for single polarizations (middle panel) or when averaged over 162 polarization vectors with endpoints maximally uniformly distributed on a sphere. We show the region between the 20th and the 45th harmonic (with one harmonic corresponding to 0.69 eV), which is a region for which the TD-CIS methodology with heuristic ionization is expected to be fairly accurate. When only a single laser polarization in the molecular plane along z is used (see the upper panel of the figure for the coordinate system), the most striking difference between cis and trans is that the former exhibits both odd and even harmonics, while the latter shows odd harmonics only. This is due to the absence of an inversion center or a symmetry plane in the (x,y)-plane, for the cis molecule. In the rotationally averaged cases, we observe

that both for cis- and trans-DCE, now only odd harmonics are seen, in agreement with experiment. The emission of only odd harmonics also for cis is again a consequence of the rotational averaging as discussed above, which in the end annihilates even harmonics for cis due to z-polarization, by a corresponding field vector in exactly opposite direction. Further, HHG spectra of cis- and trans-DCE are different, even if averaged, which also agrees with experiment. However, the quantitative agreement with experiment is not very good as outlined in Ref. 37; there, also reasons have been given why this may be so. On the other hand, calculations like those shown in Fig. 6 confirm already that HHG spectra can indeed be a valuable tool to discriminate organic isomers, even if rotational averaging washes out larger differences due to distinct molecular symmetry elements. In passing we note that in Ref. 37, also time-resolved HHG spectra have been computed, exhibiting even clearer differences between molecular isomers.

8. Conclusions and outlook

In this work, correlated, systematically improvable wavefunction methods for ultrafast electronic dynamics in molecular systems were reviewed, along with selected applications. Specifically, TD-CI and MCTDHF (or TD-CASSCF) methods were considered, the former also in the context of several extensions: The modeling of random orientations of driven molecules, the design of optimal pulses by optimal control theory and stochastic pulse optimization, the approximate treatment of ionization losses during short-pulse excitation by absorbing boundaries in energy or real space, and, finally, the treatment of energy and phase relaxation in driven, "open" many-electron systems within open-system density matrix theory. We argued that TD-CI in particular, is a powerful, economic and fairly accurate tool to treat electron dynamics in laser-stimulated molecules, even polyatomic ones. While not explicitly demonstrated here but elsewhere (see, e.g., Refs. 32, 46), we mention again that TD-CI has no problems with correctly accounting for seemingly simple situations arising in laser science, such as level inversion by π-pulses, or, more generally, the occurrence of Rabi oscillations. This is in contrast to other popular methods to treat N-electron dynamics which are based on nonlinear equations of motion, such as RT-TD-DFT.

Among the applications, we first considered the creation of electronic wavepackets by laser pulse excitation, and the importance of correlation

effects during this process. We also mentioned that the "Hartree-Fock state," a central concept in stationary quantum chemistry can be viewed as a wavepacket in the time-dependent context. We demonstrated that the occurrence/reappearance of electron correlation proceeds on the time-scale of a few tens of attoseconds in molecules, and we speculated on the possibility to design such a HF state by an optimally controlled laser pulse. More generally, optimal pulses may serve to control the entanglement of electrons. We also demonstrated that HHG spectra of molecules are accessible by TD-CI, even if Gaussian, atom-centered basis functions are used (with some reservations concerning very high harmonics, though). We also demonstrated that one may "control" HHG spectra of molecules, through the exciting laser, or by isomerization of the molecule. Since HHG radiation is the basis for tailoring attosecond pulses, both routes (the "optical" and the "chemical" one), may also be useful to control attosecond pulse generation.

As an "outlook" we only mention the following: Numerous theoretical methods, too many to be presented here, are currently being developed to describe electronic dynamics in molecules and to actively control them. Together with the enormous progress in laser physics and experiment, a new field seems to emerge: Molecular attochemistry.

Acknowledgments

We are very grateful to H.B. Schlegel (Wayne State University) for access to the TD-CIS/CAP method and computer time at the Wayne State University's computing grid, and for most fruitful discussions. We are further grateful to the Deutsche Forschungsgemeinschaft (DFG) for financial support through projects Sa 547/15-1 and Kl 1387/5-1.

References

1. Corkum, P. B.; Krausz, F. Attosecond Science. *Nat. Phys.* **2007**, *3*, 381–387.
2. Dantus, M.; Rosker, M. J.; Zewail, A. H. Real-Time Femtosecond Probing of "Transition States" in Chemical Reactions. *J. Chem. Phys.* **1987**, *87*(4), 2395–2397.
3. McPherson, A.; Gibson, G.; Jara, H.; Johann, U.; Luk, T. S.; McIntyre, I. A.; Boyer, K.; Rhodes, C. K. Studies of Multiphoton Production of Vacuum-Ultraviolet Radiation in the Rare Gases. *J. Opt. Soc. Am. B4* **1987**, *4*, 595–601.
4. Schmidt, C.; Pertot, Y.; Balciunas, T.; Zinchenko, K.; Matthews, M.; Wörner, H. J.; Wolf, J. P. High-order Harmonic Source Spanning up to the Oxygen K-edge Based on Filamentation Pulse Compression. *Opt. Express* **2018**, *26*(9), 11834–11842.
5. Midorikawa, K. High-order Harmonic Generation and Attosecond Science. *Jpn. J. Appl. Phys.* **2011**, *50*, 090001.
6. Gaumnitz, T.; Jain, A.; Pertot, Y.; Huppert, M.; Jordan, I.; Ardana-Lamas, F.; Wörner, H. J. Streaking of 43-attosecond Soft-X-Ray Pulses Generated by a Passively CEP-Stable Mid-infrared Driver. *Opt. Express* **2017**, *25*(22), 27506–27518.

7. Kanai, T.; Minemoto, S.; Sakai, H. Quantum Interference During High-order Harmonic Generation from Aligned Molecules. *Nature* **2005**, *435*, 470.
8. McFarland, B. K.; Farrell, J. P.; Bucksbaum, P. H.; Gühr, M. High Harmonic Generation from Multiple Orbitals in N_2. *Science* **2003**, *322*, 1232.
9. Rupenayan, A.; Kraus, P. M.; Schneider, J.; Wörner, H. J. Quantum Interference and Multielectron Effects in High Harmonic Spectra of Polar Molecules. *Phys. Rev. A* **2013**, *87*, 031401(R).
10. Wong, M. C. H.; Brichta, J. P.; Spanner, M.; Patchkovskii, S.; Bhardwaj, V. R. High-harmonic Spectroscopy of Molecular Isomers. *Phys. Rev. A* **2011**, *84*, 051403.
11. Marangos, J. P. Development of High Harmonic Generation Spectroscopy of Organic Molecules and Biomolecules. *J. Phys. B* **2016**, *49*, 132001.
12. Cireasa, R.; Boguslavskiy, A. E.; Pons, B.; Wong, M. C. H.; Descamps, D.; Petit, S.; Ruf, H.; Thiré, N.; Ferré, A.; Suarez, J.; Higuet, J.; Schmidt, B. E.; Alharbi, A. F.; Légaré, F.; Blanchet, V.; Fabre, B.; Patchkovskii, S.; Smirnova, O.; Mairesse, Y.; Bhardwaj, V. R. Probing Molecular Chirality on a Sub-femtosecond Timescale. *Nat. Phys.* **2015**, *11*, 655.
13. Yuan, K. J.; Lu, H.; Bandrauk, A. D. High-order-Harmonic Generation in Molecular Sequential Double Ionization by Intense Circularly Polarized Laser Pulses. *Phys. Rev. A* **2015**, *92*, 023415.
14. Gordon, A.; Kärtner, F. X.; Rohringer, N.; Santra, R. Role of Many-electron Dynamics in High Harmonic Generation. *Phys. Rev. Lett.* **2006**, *96*, 223902.
15. Luppi, E.; Head-Gordon, M. The Role of Rydberg and Continuum Levels in Computing High Harmonic Generation Spectra of the Hydrogen Atom Using Time-Dependent Configuration Interaction. *J. Chem. Phys.* **2013**, *139*, 164121.
16. White, A. F.; Heide, C. J.; Saalfrank, P.; Head-Gordon, M.; Luppi, E. Computation of High-Harmonic Generation Spectra of the Hydrogen Molecule Using Time-dependent Configuration-interaction. *Mol. Phys.* **2016**, *114*(7–8), 947–956.
17. Schönborn, J. B.; Saalfrank, P.; Klamroth, T. Controlling the High Frequency Response of H_2 by Ultra-short Tailored Laser Pulses: A Time-dependent Configuration Interaction Study. *J. Chem. Phys.* **2016**, *144*(4), 044301.
18. Koushki, A. M.; Sadighi-Bonabi, R.; Mohsen-Nia, M.; Irani, E. The Control of Quantum Trajectories on the High-order Harmonic Generation of CO and N_2 Molecules in the Presence of a Low Frequency Field. *J. Chem. Phys.* **2018**, *148*, 144306.
19. Koushki, A. M.; Sadighi-Bonabi, R.; Mohsen-Nia, M.; Irani, E. Controlling the Multi-electron Dynamics in the High-order Harmonic Spectrum of N_2O Molecules Using TDDFT. *J. Chem. Phys.* **2018**, *148*, 234303.
20. Kato, T.; Kono, H. Time-dependent Multiconfiguration Theory for Electronic Dynamics of Molecules in an Intense Laser Field. *Chem. Phys. Lett.* **2004**, *392*, 533.
21. Zanghellini, F.; Kitzler, M.; Fabian, C.; Brabec, T.; Scrinzi, A. A MCTDHF Approach to Multi-electron Dynamics in Laser Fields. *Laser Phys.* **2003**, *13*, 1064.
22. Hochstuhl, D.; Bonitz, M. Two-photon Ionization of Helium Studied with the Multiconfigurational Time-dependent Hartree-Fock Method. *J. Chem. Phys.* **2011**, *134*(8), 084106.
23. Nest, M.; Klamroth, T.; Saalfrank, P. The Multiconfiguration Time-dependent Hartree-Fock Method for Quantum Chemical Calculations. *J. Chem. Phys.* **2005**, *122*(12), 124102.
24. Pont, F. M.; Bande, A.; Cederbaum, L. S. Controlled Energy-selected Electron Capture and Release in Double Quantum Dots. *Phys. Rev. B* **2013**, *88*, 241304.
25. Rohringer, N.; Peter, S.; Burgdörfer, J. Calculating State-to-state Transition Probabilities Within Time-dependent Density-functional Theory. *Phys. Rev. A* **2006**, *74*, 042512.

26. Fuks, J. J.; Helbig, N.; Tokatly, I.; Rubio, A. Nonlinear Phenomena in Time-dependent Density-functional Theory: What Rabi Oscillations Can Teach Us. *Phys. Rev. B* **2011**, *84*, 075107.
27. Raghunathan, S.; Nest, M. The Lack of Resonance Problem in Coherent Control with Real-time Time-dependent Density Functional Theory. *J. Chem. Theory Comput.* **2012**, *8*, 806.
28. Castro, A.; Werschnik, J.; Gross, E. K. U. Controlling the Dynamics of Many-electron Systems from First Principles: A Combination of Optimal Control and Time-dependent Density-functional Theory. *Phys. Rev. Lett.* **2012**, *109*, 153603.
29. Raghunathan, S.; Nest, M. Coherent Control and Time-dependent Density Functional Theory: Towards Creation of Wave Packets by Ultrashort Laser pulses. *J. Chem. Phys.* **2012**, *136*, 064104.
30. Foresman, J. B.; Head-Gordon, M.; Pople, J. A.; Frisch, M. J. Toward a Systematic Molecular Orbital Theory for Excited States. *J. Phys. Chem.* **1992**, *96*(1), 135–149.
31. Klamroth, T. Laser-driven Electron Transfer Through Metal-insulator-metal Contacts: Time-dependent Configuration Interaction Singles Calculations for a Jellium Model. *Phys. Rev. B* **2003**, *68*, 245421.
32. Krause, P.; Klamroth, T.; Saalfrank, P. Time-dependent Configuration-interaction Calculations of Laser-pulse-driven Many-electron dynamics: Controlled Dipole Switching in Lithium Cyanide. *J. Chem. Phys.* **2005**, *123*(7), 074105.
33. Pauncz, R. *Spin Eigenfunctions: Construction and Use*. Plenum, New York, 1979.
34. Krause, P.; Klamroth, T.; Saalfrank, P. Molecular Response Properties from Explicitly Time-dependent Configuration Interaction Methods. *J. Chem. Phys.* **2007**, *127*(3), 034107.
35. Kvaal, S. Ab Initio Quantum Dynamics Using Coupled-Cluster. *J. Chem. Phys.* **2012**, *136*(19), 194109.
36. Huber, C.; Klamroth, T. Explicitly Time-dependent Coupled Cluster Singles Doubles Calculations of Laser-driven Many-electron Dynamics. *J. Chem. Phys.* **2011**, *134*(5), 054113.
37. Bedurke, F.; Klamroth, T.; Krause, P.; Saalfrank, P. Discriminating Organic Isomers by High Harmonic Generation: A Time-dependent Configuration Interaction Singles Study. *J. Chem. Phys.* **2019**, *150*, 234114.
38. Ketchum, E. A.; Tolson, R. H. Onboard Star Identification Without a Priori Attitude Information. *J. Guid. Control Dyn.* **1995**, *18*, 242–246.
39. Kosloff, R.; Rice, S. A.; Gaspard, P.; Tersigni, S.; Tannor, D. J. Wavepacket Dancing: Achieving Chemical Selectivity by Shaping Light Pulses. *Chem. Phys.* **1989**, *139*, 201.
40. Shi, S.; Rabitz, H. Quantum Mechanical Optimal Control of Physical Observables in Microsystems. *J. Chem. Phys.* **1990**, *92*, 364.
41. Klamroth, T. Optimal Control of Ultrafast Laser Driven Many-electron Dynamics in a Polyatomic Molecule: N-methyl-6-quinolone. *J. Chem. Phys.* **2006**, *124*, 144310.
42. Klamroth, T.; Kröner, D. Stereoselective Isomerization of an Ensemble of Adsorbed Molecules with Multiple Orientations: Stochastic Pulse Optimization. *J. Chem. Phys.* **2008**, *129*, 234701.
43. Serban, I.; Werschnik, J.; Gross, E. K. U. Optimal Control of Time-dependent Targets. *Phys. Rev. A* **2005**, *71*, 053810.
44. Beyvers, S.; Ohtsuki, Y.; Saalfrank, P. Optimal Control in a Dissipative System: Vibrational Excitation of CO/Cu(100) by IR Pulses. *J. Chem. Phys.* **2006**, *124*, 234706.
45. Tremblay, J. C. Laser Control of Molecular Excitations in Stochastic Dissipative Media. *J. Chem. Phys.* **2011**, *134*, 174111:1–16.
46. Klinkusch, S.; Saalfrank, P.; Klamroth, T. Laser-induced Electron Dynamics Including Photoionization: A Heuristic Model Within Time-dependent Configuration Interaction Theory. *J. Chem. Phys.* **2009**, *131*, 114304.

47. Schlegel, H. B.; Smith, S. M.; Li, X. Electronic Optical Response of Molecules in Intense Fields: Comparison of TD-HF, TD-CIS, and TD-CIS(D) Approaches. *J. Chem. Phys.* **2007**, *126*(24), 24411013.
48. Krause, P.; Sonk, J. A.; Schlegel, H. B. Strong Field Ionization Rates Simulated with Time-dependent Configuration Interaction and an Absorbing Potential. *J. Chem. Phys.* **2014**, *140*(17), 174113.
49. Coccia, E.; Assaraf, R.; Luppi, E.; Toulouse, J. Ab initio Lifetime Correction to Scattering States for Time-dependent Electronic-structure Calculations with Incomplete Basis Sets. *J. Chem. Phys.* **2017**, *147*(1), 014106.
50. Krause, P.; Schlegel, H. B. Strong-field Ionization Rates of Linear Polyenes Simulated with Time-dependent Configuration Interaction with an Absorbing Potential. *J. Chem. Phys.* **2014**, *141*(17), 174104.
51. Krause, P.; Schlegel, H. B. Angle-dependent Ionization of Small Molecules by Time-dependent Configuration Interaction and an Absorbing Potential. *J. Phys. Chem. Lett.* **2015**, *6*, 2140–2146.
52. Tremblay, J. C.; Klamroth, T.; Saalfrank, P. Time-dependent Configuration Interaction Calculations of Laser-driven Dynamics in Presence of Dissipation. *J. Chem. Phys.* **2008**, *129*, 084302.
53. Klinkusch, S.; Tremblay, J. C. Resolution-of-identity Stochastic Time-dependent Configuration Interaction for Dissipative Electron Dynamics in Strong Fields. *J. Chem. Phys.* **2016**, *144*(18), 184108.
54. Wang, H.; Möhle, T.; Kühn, O.; Bokarev, S. Ultrafast Dissipative Spin-state Dynamics Triggered by X-ray Pulse Trains. *Phys. Rev. A* **2018**, *98*, 013408.
55. Lindblad, G. On the Generators of Quantum Dynamical Semigroups. *Commun. Math. Phys.* **1976**, *48*, 119.
56. Gorini, V.; Kossakowski, A.; Sudarshan, E. C. G. Properties of Quantum Markovian Master equations. *J. Math. Phys.* **1976**, *17*, 821.
57. Tremblay, J. C.; Krause, P.; Klamroth, T.; Saalfrank, P. Time-dependent Response of Dissipative Electron Systems. *Phys. Rev. A* **2010**, *81*, 063420.
58. Hermann, G.; Tremblay, J. C. Laser-driven Hole Trapping in a Ge/Si Core-shell Nanocrystal: An Atomistic Configuration Interaction Perspective. *J. Phys. Chem. C* **2015**, *119*, 25606.
59. Tremblay, J. C.; Klamroth, T.; Klinkusch, S.; Saalfrank, P. Dissipative Many-electron Dynamics of Ionizing Systems. *J. Chem. Phys.* **2011**, *134*, 044311.
60. Nest, M.; Padmanaban, R.; Saalfrank, P. Time-dependent Approach to Electronically Excited States of Molecules with the Multi-configuration Time-dependent Hartree-Fock Method. *J. Chem. Phys.* **2007**, *126*, 214106.
61. Remacle, F.; Nest, M.; Levine, R. D. Laser Steered Ultrafast Quantum Dynamics of Electrons in LiH. *Phys. Rev. Lett.* **2007**, *99*, 183902.
62. Nest, M.; Ludwig, M.; Ulusoy, I.; Klamroth, T.; Saalfrank, P. Electron Correlation Dynamics in Atoms and Molecules. *J. Chem. Phys.* **2013**, *138*, 164108.
63. Klinkusch, S. Simulations of Laser-driven Correlated Many-electron Dynamics in Molecular Systems (Ph.D. thesis); University of Potsdam, Potsdam, Germany, **2011**.
64. Lünnemann, S.; Kuleff, A. I.; Cederbaum, L. S. Ultrafast Charge Migration in 2-Phenylethyl-N,N-dimethylamine. *Chem. Phys. Lett.* **2008**, *450*(4–6), 232–235.
65. Trabattoni, A.; Galli, M.; Lara-Astiaso, M.; Palacios, A.; Greenwood, J.; Tavernelli, I.; Decleva, P.; Nisoli, M.; Martín, F.; Calegari, F. Charge Migration in Photo-ionized Aromatic Amino Acids. *Phil. Trans. R. Soc. A377*, 20170472.
66. Kraus, P. M.; Mignolet, B.; Baykusheva, D.; Rupenyan, A.; Horný, L.; Penka, E. F.; Grassi, G.; Tolstikhin, O. I.; Schneider, J.; Jensen, F.; Madsen, L. B.; Bandrauk, A. D.; Remacle, F.; Wörner, H. J. Measurement and Laser Control of Attosecond Charge Migration in Ionized Iodoacetylene. *Science* **2015**, *350*, 790–795.

67. Corkum, P. B. Plasma Perspective on Strong Field Multiphoton Ionization. *Phys. Rev. Lett.* **1993**, *71*, 1994–1997.
68. Lewenstein, M.; Balcou, P.; Ivanov, M. Y.; L'Huillier, A.; Corkum, P. B. Theory of High-harmonic Generation by Low-frequency Laser Fields. *Phys. Rev. A* **1994**, *49*, 2117.
69. Lein, M.; Hay, N.; Velotta, R.; Marangos, J. P.; Knight, P. L. Interference Effects in High-order Harmonic Generation with Molecules. *Phys. Rev. A* **2002**, *66*, 023805.
70. Labeye, M.; Zapata, F.; Coccia, E.; Véniard, V.; Toulouse, J.; Caillat, J.; Taieb, R.; Luppi, E. Optimal Basis Set for Electron Dynamics in Strong Laser Fields: The Case of Molecular Ion H_2^+. *J. Chem. Theor. Comput.* **2018**, *14*, 5846.
71. Bachau, H.; Cormier, E.; Decleva, P.; Hansen, J. E.; Martin, F. Applications of B-Splines in Atomic and Molecular Physics. *Rep. Prog. Phys.* **2001**, *64*, 1815.
72. Chang, Z.; Rundquist, A.; Wang, H.; Christov, I.; Kapteyn, H. C.; Murnane, M. M. Temporal Phase Control of Soft-X-ray Harmonic Emission. *Phys. Rev. A* **1998**, *58*, R30–R33.
73. Lee, D. G.; Kim, J. H.; Hong, K. H.; Nam, C. H. Coherent Control of High-order Harmonics with Chirped Femtosecond Laser Pulses. *Phys. Rev. Lett.* **2001**, *87*, 243902.
74. Winterfeldt, C.; Spielmann, C.; Gerber, G. *Colloquium*: Optimal Control of High-harmonic Generation. *Rev. Mod. Phys.* **2008**, *80*(1), 117–140.
75. Balogh, E.; Bódi, B.; Tosa, V.; Goulielmakis, E.; Varjú, K.; Dombi, P. Genetic Optimization of Attosecond-pulse Generation in Light-field Synthesizers. *Phys. Rev. A* **2014**, *90*, 023855.
76. Castro, A.; Rubio, A.; Gross, E. K. U. Enhancing and Controlling Single-atom High-harmonic Generation Spectra: A Time-dependent Density-functional Scheme. *Eur. Phys. J. B* **2015**, *88*, 191.